Low Temperature Physics/Fizika Nizkikh Temperatur, 2018, v. 44, No. 9, pp. 1233–1240

Amplitude-dependent internal friction in AZ31 alloy sheets submitted to accumulative roll bonding

Z. Trojanová, Z. Drozd, P. Lukáč, and P. Minárik

Faculty of Mathematics and Physics, Charles University, Prague, Ke Karlovu 3, 121 16 Praha 2, Czech Republic
E-mail: ztrojan@met.mff.cuni.cz

J. Džugan and K. Halmešová

Comtes FHT, Průmyslová 996, 334 41 Dobřany, Czech Republic

Received March 19, 2018, published online July 26, 2018

Fine grained magnesium alloy AZ31 sheets were submitted to the accumulative roll bonding (ARB). After ARB, the microstructure of samples was refined, and the sheets exhibited pronounced texture. The amplitude-dependent internal friction (ADIF) was measured at room temperature. Microstructure changes as the increased dislocation density, grain size refinement, twins, and texture influenced the ADIF. A significant anisotropy of the properties was observed. Experimental results are discussed on the base of physical mechanisms responsible for internal friction.

Keywords: magnesium alloy, accumulative roll bonding, internal friction, dislocations, twinning, texture.

1. Introduction

Magnesium alloys with their high specific strength and low weight are used as structural materials in different applications. They have suitable mechanical and excellent damping [1]. Magnesium wrought alloys, such as for instant AZ31, are needed for applications where their weight is important. It is well known that the mechanical properties of Mg alloys depend very sensitive on their microstructure [2]. Grain refinement is an effective way leading to a higher strength and ductility. Different procedures have been used for the grain refinement. Thus, extrusion of samples causes grain refinement and may produce texture and then anisotropy of mechanical properties [3].

In recent years, methods of severe plastic deformation (SPD) have attracted interest of many researchers investigating also properties of magnesium alloys [4]. Very often, equal channel angular pressing (ECAP) and high pressure torsion (HPT) are used to influence the microstructure. Rarely, accumulative roll bonding technique is used. In this processing, a sheet is rolled to 50% thickness, cut to two halves that are connected and then again rolled [5]. In contrast to extrusion and/or rolling, the ECAP and HPT processing affect significantly the microstructure of Mg; not only grains are refinement but also the total dislocation change depending on conditions of processing. Many papers describing the effect of ECAP on the mechanical properties of AZ31 magnesium alloys have been presented [6–8]. On the other hand, very few experiments on the influence of ARB on properties of AZ31 were conducted. It is important to mention that also twins and texture changes can be induced in samples undergone to SPD processing [9–11].

Microstructure changes have a significant influence on internal friction. Damping of materials depends on microstructure, stress, temperature or frequency. The internal friction is a result of motion of structural defects such as point defects, dislocations, twins or grain boundaries. Conversely internal friction measurements can be used to study changes in the microstructure or the density and mobility of structural defects.

The purpose of the present study is to investigate the effect of microstructure modifications, introduced by the accumulative roll bonding into AZ31 alloy sheets, on strain amplitude-dependent internal friction with the focus on the mechanisms which are responsible for these changes.

2. Experimental procedure

Commercially available sheets from a magnesium alloy AZ31 were used in this study. The chemical composition (in wt%) of the alloy is introduced in Table 1.

Table 1. Chemical composition of the alloy studied (in wt.%)

Material	Al	Zn	Mn	Si	Fe	Ce	Mg
AZ31_RS	3.2	1.3	0.4	0.015	0.03	0.06	Bal.

The accumulative roll bonding of AZ31 magnesium alloy was performed using four high-rolling mill configuration. Two strips with initial thickness of 2 mm were degreased with acetone, then wire brushed and fastened along one side. These steps ensured conditions to achieve good-quality joint. Prior to rolling the sheets were annealed at 400 °C for 15 min. At lower temperatures, material failed to bond. The rolling speed was 0.4 mm/s and the ARB experiments were carried out without a lubricant. The rolling reduction was 50% in the thickness per each rolling cycle. Two passes through the rolling mill were successfully realized. Samples for the internal friction measurements were cut from the sheets so that the longest axis of the sample was either parallel (L-samples) or transversal (T-samples) to the rolling direction. Samples from the ARB sheets will be depicted hereafter as ARB_0 (original sheet), ARB_1 (after the first ARB pass) and ARB_2 (after the two ARB passes).

Microstructure of samples was studied using a light microscope Neophot and scanning electron microscope (SEM) Tescan. The texture analysis was performed in the ZEISS Auriga Compact microscope equipped with EDAX EBSD camera and special software, utilized for EBSD observations.

Internal friction measurements were carried out on bending beams (86 mm long, 10 mm wide and 2.3 mm thick) at room temperature. The internal friction was obtained by the measurement of the logarithmic decrement of free decaying bending beam vibrations in the resonant frequency. Details of the apparatus were described in [12]. The typical resonant frequency exhibited about 22 Hz. The logarithmic decrement, δ, was estimated directly from the definition according the exponential law

$$A(t) = A_0 \exp(-\delta t / \tau_p), \quad (1)$$

where A_0 is the required amplitude, t is the time and τ_p is the period of vibrations. The signal amplitude is proportional to the strain amplitude, ε. The amplitude dependences of the decrement were measured from the maximum amplitude towards to the lower amplitudes.

3. Results and discussion

3.1. Microstructure of sheets

Light micrograph of the as-received L-sample, taken from the sheet surface, is reported in Fig. 1. Dark particles are typical features of the microstructure. Bigger particles are elongated in the rolling direction; smaller particles decorate the grain boundaries. Chemical analysis of particles showed that these particles containing Al and Mn are very probably Al_8Mn_5 precipitates which were described in the literature by several authors [13,14]. No precipitates $Mg_{17}Al_{12}$ typical for Mg–Al–Zn alloys were observed in the microstructure. This was probably due to a higher processing temperature during the rolling process (400 °C).

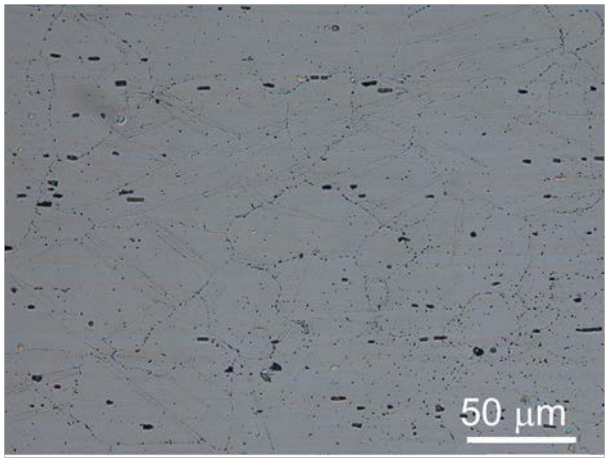

Fig. 1. Microstructure of ARB_0 sample, taken from the sheet surface.

Traces of the bonding between sheets are visible in Fig. 2 indicated by the arrows. This bonding emerged strong enough, no delamination of samples was observed even during plastic deformation at elevated temperatures [15]. Good bonding may be achieved as a result of dynamic recrystallization (DRX) [16].

The effect of the ARB on the sheet microstructure is shown in Fig. 3 by the means of EBSD. The micrograph of the as-received material is shown in Fig. 3(a). Large grains of size ~100 μm are surrounded by smaller ones; many twins are typical feature of the microstructure. The first rolling pass refined the grains. The grain size decreased ten times down to ~10 μm as it is obvious from Fig. 3(b). The highest area fraction had grains of 4–5 μm in diameter. On the other hand, bigger grains 40–60 μm remained in the microstructure. The fraction of high-angle grain boundaries was particularly high ~0.8. Some bigger grains exhibit changing colour, which indicates the high lattice distortion due to high deformation energy stored in the grains. The microstructure of the ARB_2 is presented in Fig. 3(c). The

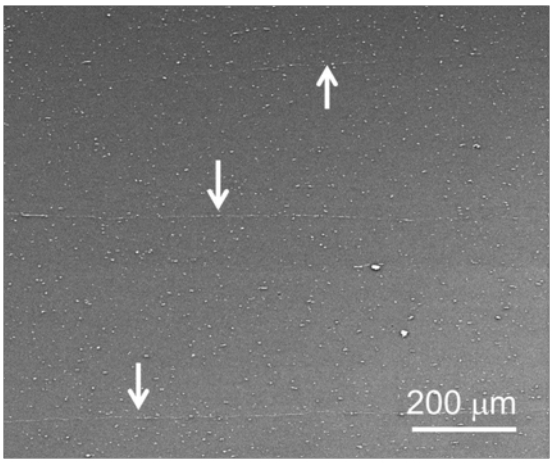

Fig. 2. SEM micrograph of the ARB_2 sample showing joining of sheets indicated by arrows.

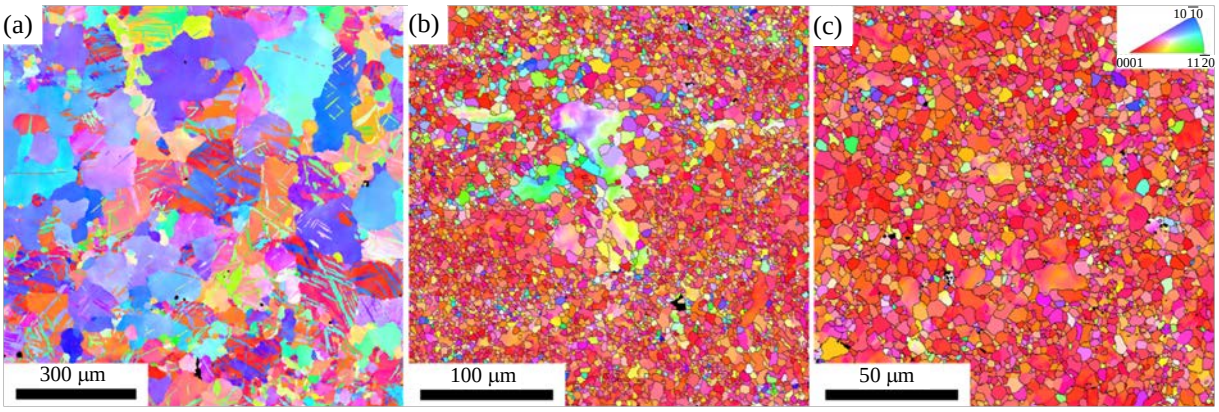

Fig. 3. (Color online) EBSD microstructure of samples ARB_0 (a), ARB_1 (b) and ARB_2 (c).

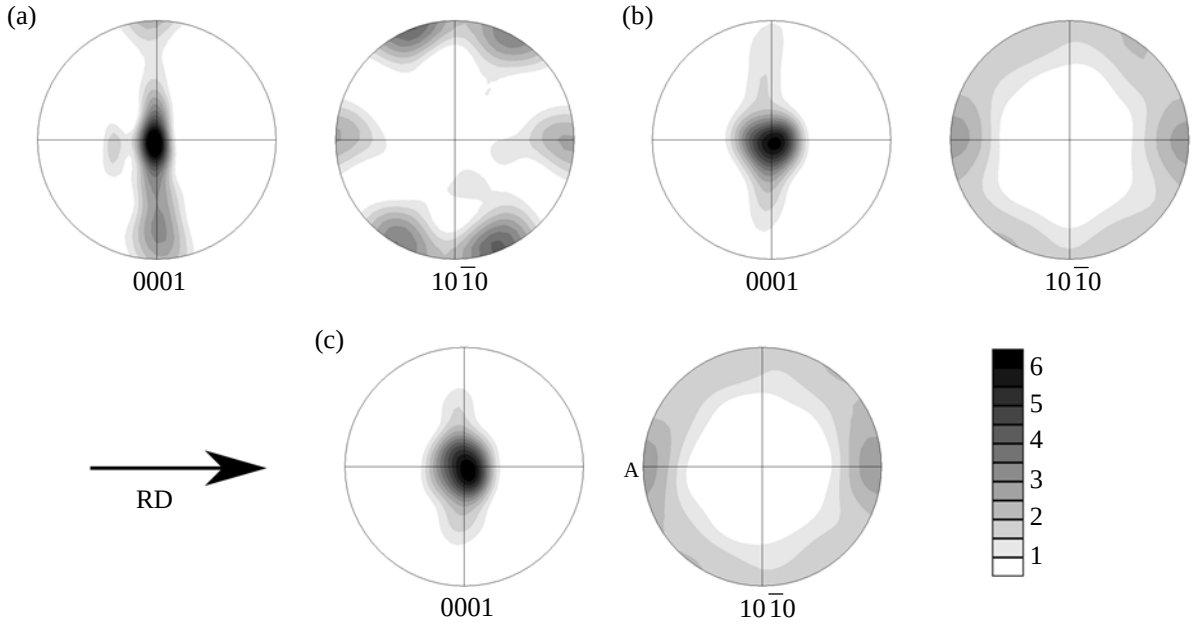

Fig. 4. Pole figures of ARB_0 sample (a), ARB_1 sample (b) and ARB-2 sample (c).

microstructure is more homogeneous, the bigger grains (> 30 μm) vanished. The mean grain size again decreased down to ~7.6 μm in diameter, but the highest area fraction was still represented by grains of 4–5 μm.

Revealing red colour in the pictures presented in Figs. 3(a)–(c) indicates existing texture of rolled sheets. EBSD pole figures are shown in Fig. 4. The texture can be characterized as a fibre texture with the **c**-axis perpendicular to the sheet surface. Crystallographic texture was improved during the ARB process in the first and second rolling pass. The distribution of basal poles shows a basal pole tilted away from the normal direction towards the transverse direction, as can be seen in Fig. 4.

3.2. Amplitude-dependent internal friction

The logarithmic decrement, δ, is plotted against the strain amplitude, ε, Fig. 5 for L-sample and T-sample. The dependences can be divided as obvious into two regions: an ampli-

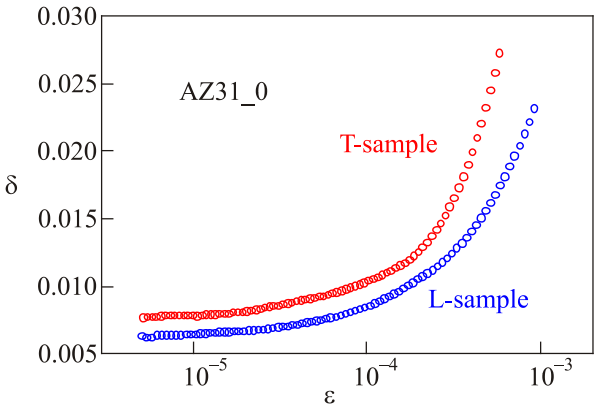

Fig. 5. Amplitude dependences of decrement measured for L-sample and T-sample.

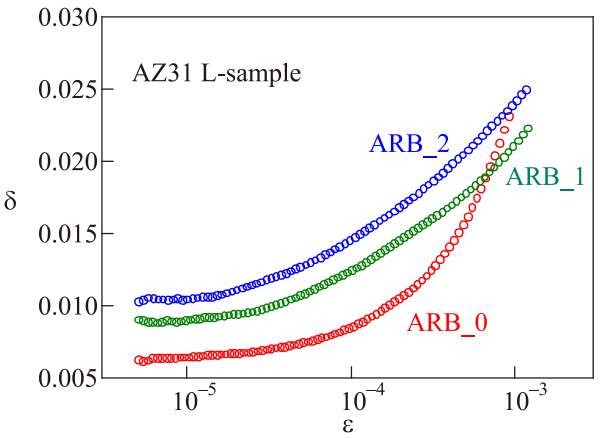

Fig. 6. (Color online) Amplitude dependences of decrement measured for L-sample after ARB rolling.

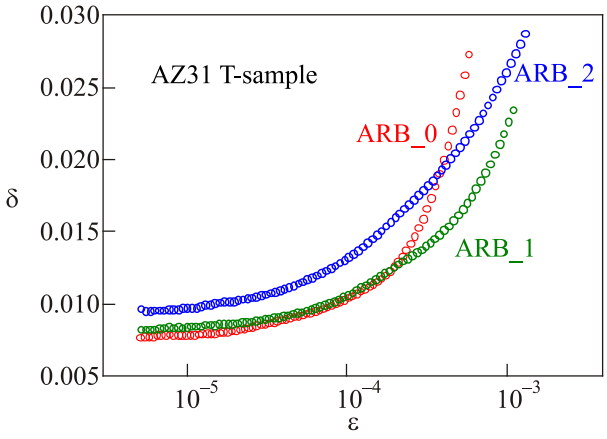

Fig. 7. (Color online) Amplitude dependences of decrement measured for T-sample after ARB rolling.

tude-independent (or slightly depending on strain amplitude) part, δ_0, of the decrement found for smaller strain amplitudes and the region of higher amplitudes where decrement, $\delta(\varepsilon)$, rapidly increases with strain amplitude, i.e., δ can be expressed as

$$\delta = \delta_0 + \delta_H(\varepsilon). \qquad (2)$$

From Fig. 5, it is obvious that the decrement values estimated in both regions are higher for T-sample comparing with the L-sample. Such planar plastic anisotropy of samples deformed in L and T direction is known and it was several times described in the literature [17–21]. Such planar anisotropy is not limited only on plastic properties, but it was also found for Young's modulus and the thermal expansion coefficient [22,23]. Similar results were obtained for AZ31 alloy sheet in a different apparatus as it was shown in [24]. The difference between both sample orientations was more significant, very probably due to a bigger maximum strain amplitude. The ARB process influences the decrement in both regions. It is demonstrated in Fig. 6 for L-samples and in Fig. 7 for T-samples. The shape of curves changed, and curves were shifted to higher values of the decrement especially for smaller amplitudes. The decrement component, δ_0, estimated at an amplitude $\varepsilon = 5{\cdot}10^{-6}$ was plotted as a function of rolling passes for both sample orientations (see Fig. 8). It can be seen that δ_0 component increases with increasing number of passes. This increase is more distinctive for L-samples where δ_0 increased approximately two times. On the other hand, the increase of δ_0 is only moderate.

Rolled sheets after the ARB process exhibit also a significant internal stress. Samples of both orientations were heated in a dilatometer and the thermal expansion was measured. After one cycle from room temperature up to 400 °C with a heating rate of 0.9 K/min permanent shortening of samples was estimated. This relative shortening in percent is presented in Fig. 9 for samples of both orientations. While the shortening of T-samples was more or less the same, only slightly dependent on the number of passes; shortening of L-sample increases rapidly with increasing number of rolling passes. This result indicates that the internal stresses are higher in samples with the longest axis parallel to the rolling direction.

While internal friction in the amplitude-independent part may be done by several mechanisms (dislocation internal

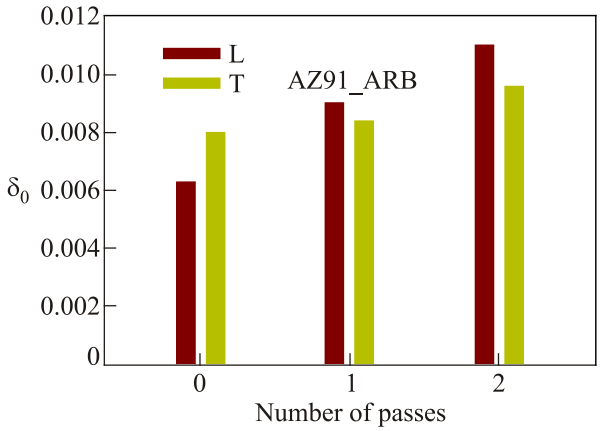

Fig. 8. Amplitude component, δ_0, of decrement estimated in L- and T-samples after ARB passes.

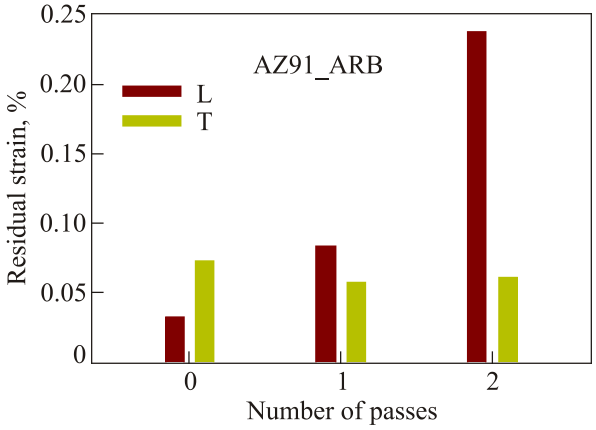

Fig. 9. Permanent strain depending on number of ARB passes measured after thermal cycle of L- and T-sample.

friction, grain boundary sliding, thermoelastic effect), the amplitude-dependent part is only due to presence of dislocation in the material. The thermoelastic loss may be observed in the bending reed or a thin beam during vibrations at low frequencies [25,26]. Damping can occur by heat flow from the hotter (compressed) parts to the cooler (extended) parts of the sample. For the thermoelastic internal friction following relationship may be written

$$\delta_{TE} = \Delta_T \frac{f f_0}{f^2 + f_0^2}, \tag{3}$$

where Δ_T is the relaxation strength, f is the measuring frequency and f_0 is the frequency at which the maximum of the thermoelastic damping can be observed. Both quantities f_0 and Δ_T depend on thermal properties of the sample material and its geometry:

$$f_0 = \pi / 2d^2 \rho_m C_p, \quad \Delta_T = \alpha^2 E_u T / \rho_m C_p, \tag{4}$$

where κ is the thermal conductivity, ρ_m is the material density, α is the thermal expansion coefficient, T is the absolute temperature, d is the sample thickness, E_U is unrelaxed Young's modulus, and C_p is the specific heat at constant pressure. Taking for κ = 76 W/(m·K), d = 2.3 mm, ρ_m = = 1738 kg/m^3, C_p = 1010 J/(kg·K), E_U = 44 GPa and α = = 26.5·10^{-6} K^{-1} [27], we obtain at room temperature for f_0 = 12.85 Hz and Δ_T = 0.0052. Although the thermal properties depend slightly on the sample orientation and number of passes, it is reasonable to consider that the contribution to the internal friction value coming from the thermoelastic effect will be for all samples approximately the same of δ_{TE} = 0.0023.

In the vibrating string model the dislocation amplitude-independent decrement component can be written as [28,29]

$$\delta_0 = \frac{\Omega B \rho \ell^4 \omega}{E_L b^2}, \tag{5}$$

where Ω is an orientation factor, ρ is the dislocation density, B is the coefficient of dislocation friction and E_L is the tension in a dislocation line, b is the magnitude of the Burgers vector of dislocations and ℓ is length of shorter dislocation segments between weak pinning points which may be point defects or their small clusters.

The breakaway of dislocations from the weak pinning points may occur when the force impacting on two adjacent dislocation segments with the length ℓ_1 and ℓ_2 exceed the Cottrell energy E_C/b. Therefore, the critical stress, σ_c, for breakaway is given in the single pin approximation at zero temperature as $b\sigma_c(\ell_1 + \ell_2)/2 = |E_C|/b$. The amplitude-dependent internal friction was calculated by Granato and Lűcke [30] under simplified conditions that dislocations in a crystal form a network with the same loop length of L_N. Shorter dislocation segments pinned by the weak pinning points are statistically distributed along the longer dislocation segments. At temperatures higher than 0 K, the amplitude dependence of the logarithmic decrement may be expressed in the low-frequency limit as an exponential function in the following form:

$$\delta_H = \frac{\rho L_N^2}{6} \frac{\nu}{\omega} \left(\frac{3\pi kT}{2U_0} \right)^{1/2} \left(\frac{\ell^3 \sigma^2}{U_0 G} \right)^{1/2} \exp\left[-\frac{4}{3} \frac{U_0}{kT} \left(\frac{U_0 G}{\ell^3} \right)^{\frac{1}{2}} \frac{1}{\sigma} \right], \tag{6}$$

where G is the shear modulus, σ is the amplitude of the applied stress and ω its angular frequency, ν is the attack frequency. U_0 is the activation energy of overcoming pinning centres, k is the Boltzmann constant and T is the absolute temperature. In the formula (6), the δ_H component is an exponential function of the applied stress amplitude similar to the original formula by Granato and Lücke [28,29]. Because the stress and strain amplitudes are related by the Hooke's law, Eq. (6) may be rewritten as

$$\delta = \delta_0 + C_1 \varepsilon \exp\left(-C_2 / \varepsilon\right), \tag{7}$$

where $\varepsilon = \sigma/E$, C_1 and C_2 are parameters depending on dislocation density and length of the shorter and longer dislocation segments. Because all experiments were performed at room temperature, the activation energy may be considered in the first approximation as a constant.

The amplitude dependences of the logarithmic decrement were fitted to Eq. (7) as it is shown in Fig. 10. The correlation to the experimental points is good, R^2 = 0.998 for L-sample and R^2 = 0.992 for T-sample. Parameter C_1 was estimated C_1(L) = 18.9 and C_1(T) = 35.1. Note that the vibrating string model and dislocation dynamics were constructed for single crystals of "pure" metals. The model is highly idealized and it does not take into account interactions between dislocation loops, the fact that the line energy of dislocations depends on the dislocation type and may be affected by anisotropy [31]. In real materials (alloys), the comparison of experimental results with the the-

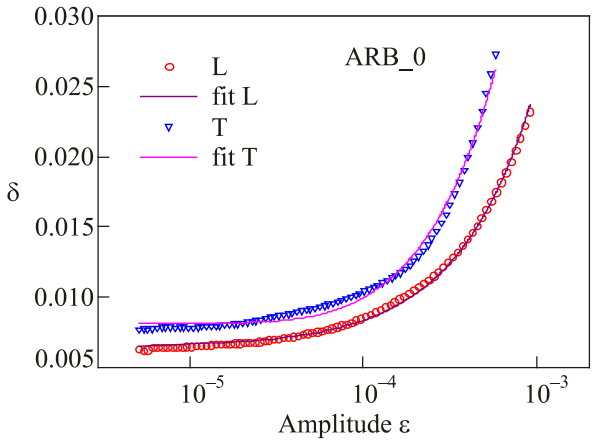

Fig. 10. (Color online) GL fit for ARB_0 samples in both orientations.

oretical model may be performed only qualitatively. Because the C_1 parameter ~ $\ell^{3/2}$, the higher value of the C_1 parameter in the T-sample indicates a higher length of dislocation segments operating in the slip plane after breakaway of shorter segments from the weak pinning points. It means that the area swept by dislocation segments is bigger in the T direction.

Many pre-existing twins in the material are documented in Fig. 2(a). These twins contribute to the amplitude-independent component of the logarithmic decrement, δ_0, very probably in both sample orientations. The idea of enhanced internal friction due to presence of twins in Mg and Mg alloys was pronounced by several authors [32–34]. They consider that the twin boundary is movable under alternating strain and it can either shrink or extent the twin width even at stresses much lower than the nucleation stress [32,33]. Watanabe *et al.* [34] studied the influence of deformation twins on internal friction in extruded pure Mg. They found that pre-deformation increased internal friction due to new twins which were formed during compressive deformation of the textured samples. Rolled sheets studied exhibit texture where basal planes are parallel to the sheet surface. The force causing the sheet vibrations impacts in the perpendicular direction to the sheet surface. In such situation, $\langle a \rangle$ dislocations are movable in (0001) basal and $\{11\bar{2}0\}$ prismatic planes. On the other hand, basal poles are split into transversal direction (see Figs. 4) in all samples. The splitting of basal poles decreases with increasing number of passes. Such type of the texture with the angular distribution of the basal poles broader in the transversal direction is favorable for mechanical twinning. Tensile experiments of samples with the stress axis in the rolling direction and transversal direction showed that the yield stress in the transversal direction is much lower than the yield stress found for rolling direction, i.e., YS(RD) = 162 MPa and YS(TD) = 85 MPa [15]. This planar plastic anisotropy was explained by the different deformation mechanisms occurring during plastic straining of both samples. While deformation process in the rolling direction is realized mainly by the dislocation motion, mechanical twinning may be consider as the significant deformation mechanism at the onset of deformation in the transversal direction. It is done by the lower critical resolved stress of twinning. Because twinning is a polar mechanism it can operate if special geometrical conditions (texture) are fulfilled [35]. Acoustic emission activity characterised by the count rate observed during tensile deformation showed a higher intensity of acoustic emission in the sample cut in the transversal direction as it is shown in Fig. 11. Note that the scale on the count rate axis is logarithmic, thus the acoustic emission in the T-sample is at the very beginning of deformation approximately ten times higher. It is valid for very low strains (stresses) in the microyielding region which corresponds with the region of the internal friction measurements. In the bending experiment the half of the sample is

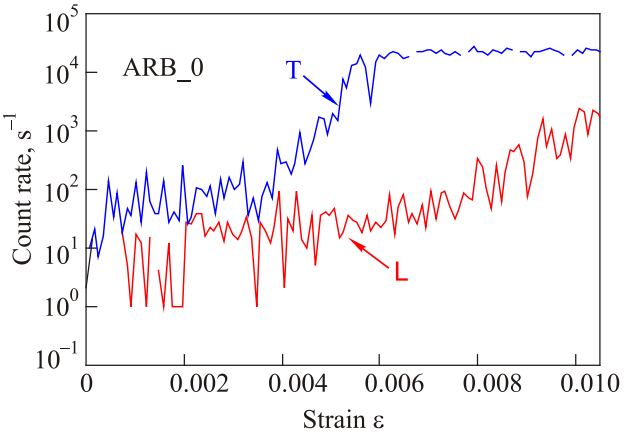

Fig. 11. (Color online) Acoustic emission activity measured during tensile deformation in samples of both orientations.

in tension while the second part of the sample is in compression. Both parts of sample are divided by the neutral plane. In the next half cycle, the situation is opposite. Taking into account results of acoustic emission measurements, we may consider that new $\{10\bar{1}2\}\langle 10\bar{1}1\rangle$ tension twins are generated during loading in measuring apparatus [36]. In the following half cycle detwinning takes place and these tension twins are erased. Huang *et al.* and Yang *et al.* found that the critical resolved stress for the twins' formation is really very low 2–2.8 MPa and tensile twins may be easily formed [37,38]. Taking in the consideration that Young's modulus for AZ31 alloy E = 44 GPa, then such stress can be achieved at the amplitudes of $\varepsilon = (4.5–6.4)\cdot 10^{-5}$. Note that in the samples exist appreciable residual tensile stresses (see Fig. 9) which can add to the applied stress and formatted the originally symmetrical tension — compression cycle into unsymmetrical.

The amplitude dependences of the logarithmic decrement measured after the first and second rolling passes are shown in Fig. 6 for L-sample and 7 for T-sample. It can be seen that the shape of curves changed. The logarithmic dependence of Eq. (7) is no more applicable for these curves. In a material submitted to SPD processing, many microstructural aspects must be taken into account. Internal friction is influenced by:

i) Decreased grain size;

ii) Increased volume of grain boundaries;

iii) Increased dislocation density;

iv) Dislocations in small angle grain boundaries;

v) Increased level of tensile residual stresses in the rolling direction.

Decreasing grain size after the first and second ARB passes is well visible in Figs. 2(b) and 2(c).

Internal friction in pure Mg and AZ31 magnesium alloy subjected to EXECAP processing was studied by Fan and co-workers [39,40]. They found increased internal friction values in the strain-independent part due to abundant mobile dislocations induced by the ECAP processing. How-

ever, the intense tangle of dislocations and significant increase of the grain boundary volume contribute to a decrease in strain-independent IF for ECA extruded Mg. The GL model is applicable only for lower strain amplitudes. Annealing at 200 and 300 °C reduced IF in the amplitude-independent part due to a decrease of dislocation density, while strain-dependent part is obviously increased. A higher dislocation density may be considered also after intense plastic deformation due to rolling. High temperature of the ARB process was the reason for the reconstruction of the grain structure via operation of the rotational dynamic recrystallization (RDX). Increased dislocation density contributes to the amplitude-independent internal friction increase. However, increased dislocation density restricts the mean free paths of dislocations and the area swept by dislocations after successful breakaway form the weak pinning points. The EBSD analysis showed that 20 % of grain boundaries are small angle grain boundaries formed by the edge dislocations. These dislocations may also contribute to the internal friction.

Trojanová *et al.* [41] studied internal friction in the microcrystalline Mg and Mg reinforced with the ceramic nanoparticles and showed that the nanoparticles were situated mainly in the grain boundaries. The amplitude-dependent component of the decrement decreased in the Mg + 3 vol.% *n*-Al_2O_3. Because of good bonding between nanoparticles and Mg matrix, these nanoparticles restricted grain boundary sliding. In a material with the grain size in the μm region, grain boundary sliding may be not excluded, and it increases the internal friction in the amplitude-independent region. On the other hand, the influence of twinning decreases with decreasing grain size. The stress necessary for twin's formation increases with the decreasing grain size, as it was shown in mechanical tests [24]. The ARB process introduced into the materials (ARB_1) and (ARB_2) new interfaces. Although the bonding at the interface is very good (no delamination of samples was not observed even at elevated temperatures), sliding in this interface may not be excluded. The interface is parallel with the sample axis in L-sample and perpendicular in the T-samples. It is reasonable to expect that the influence of this new interface will be more substantial in the L-sample.

As it was mentioned above, it is not possible to describe the amplitude dependence of decrement by the exponential function theoretically proposed by Granato and Lücke [30]. This is very probably due to complex character of internal friction in a highly deformed polycrystalline material. Several mechanisms contribute to internal friction and each of them has its specific influence on the amplitude-independent and dependent damping.

4. Conclusions

The amplitude dependences of internal friction were measured in AZ31 alloy sheets after accumulative roll bonding at room temperature. Following conclusions may be drawn from the experimental finding.

– Anelastic planar anisotropy of internal friction was observed; the logarithmic decrement was higher in rolled sheets cut perpendicular to the rolling direction than that in the samples where the longer axis was parallel to the rolling direction.

– Different loss mechanisms are responsible for this anisotropy; dislocation internal friction is the main loss mechanism in samples cut parallel with the rolling direction while in the transversal samples twin's formation and twin's boundary motion contribute to the internal friction.

– Accumulative roll bonding increased internal friction; internal friction in the highly deformed material is some complex problem where various mechanisms (dislocation internal friction, grain-boundary sliding, interface sliding) contribute to internal friction.

Acknowledgments

It is a great honour for us to have opportunity to dedicate this paper to Vasilii Dmitrievich Natsik, well known physicist theoretician, on the occasion of his 80th birthday. We wish Vasilii good health and much happiness in the years ahead.

This study was realized with the financial support of the Grant Agency of the Czech Republic under project 18-07140S.

1. R. González-Martínez, J. Göken, D. Letzig, K. Steinhoff, and K.U. Kainer, *J. Alloys Compd*. **437**, 127 (2007).
2. Q. Wang, B. Jiang, Y. Chai, B. Liu, and F. Pan, *Mater. Sci. Eng. A* **673**, 606 (2016).
3. G.-J. Huang, Q. Liu, L.-Y. Wang, R.-L. Xin, and F.-S. Pan, *Transactions of Nonferrous Metals Society of China* **18**, 170 (2008).
4. Y. Estrin and A. Vinogradov, *Acta Mater.* **61**, 782 (2013).
5. X.Y. Lou, X. M. Li, R.K. Boger, S.R. Agnew, and R.H. Wagoner, *Int. J. Plast.* **23**, 44 (2007).
6. Z. Horita, T. Fujinami, and T.G. Langdon, *Mater. Sci. Eng. A* **318**, 34 (2001).
7. R.B. Figueiredo, Z. Száraz, Z. Trojanová, P. Lukáč, and T.G. Langdon, *Scripta Mater.* **63**, 504 (2010).
8. H.K. Lin, J.C. Huang, and T.G. Langdon, *Mater. Sci. Eng. A* **402**, 250 (2005).
9. W. Chen, W. Zhang, Y. Qiao, Q. Miao, and E. Wang, *J. Alloys Compd*. **665**, 13 (2016).
10. J. A. del Valle, M.T. Pérez-Prado, and O.A. Ruano, *Mater. Sci. Eng. A* **410**, 353 (2005).
11. M.T. Pérez-Prado, J.A. del Valle, and O.A. Ruano, *Scripta Mater.* **51**, 1093 (2004).
12. Z. Trojanová, P. Lukáč, and W. Riehemann, *Mater. Sci. Eng. A* **521–522**, 314 (2009).
13. M. Ohno, D. Mirkovic, and R. Schmid-Fetzer, *Acta Mater.* **54**, 3883 (2006).

14. K.N. Braszczyńska-Malik, *J. Alloys Compd.* **477**, 870 (2009).
15. Z. Trojanová, J. Džugan, K. Halmešová, G. Németh, P. Lukáč, P. Minárik, and J. Bohlen, *Materials* **11**(1), 73 (2018).
16. Q.F. Wang, X.P. Xiao, J. Hu, W.W. Xu, X.Q. Zhao, and J.S. Zhao, *Proc. of Sino-Swedish Structural Materials Symposium* (2007), p. 167.
17. J. Balík, P. Dobroň, F. Chmelík, R. Kužel, D. Drozdenko, J. Bohlen, D. Letzig, and P. Lukáč, *Int. J. Plast.* **76**, 166 (2016).
18. J. Balík, P. Lukáč, Z. Drozd, and R. Kužel, *Int. J. Mater. Res.* **100**, 322 (2009).
19. J. Bohlen, M.R. Nürnberg, J.W. Senn, D. Letzig, and S.R. Agnew, *Acta Mater.* **55**, 2101 (2007).
20. R.K. Mishra, A.K. Gupta, P.R. Rao, A.K. Sachdev, A.M. Kumar, and A.A. Luo, *Scripta Mater.* **59**, 562 (2008).
21. Z.P. Yu, Y.H. Yan, J. Yao, C. Wang, and Q.C. Jiang, *J. Alloys Compd*. **744**, 211 (2018).
22. Z. Trojanová, K. Halmešová, J. Džugan, Z. Drozd, P. Minárik, and M. Knapek, *IOP Conf. Series: Materials Science and Engineering* **219**, 012023 (2017).
23. Z. Drozd, Z. Trojanová, K. Halmešová, J. Džugan, P. Lukáč, and P. Minárik, *Acta Physica Polonica A*, accepted for publication.
24. Z. Trojanová, P. Lukáč, J. Džugan, and K. Halmešová, *Metals* **7**, 433 (2017).
25. A.S. Novick and B.S. Berry, *Anelastic Relaxation in Crystalline Solids*, Academic Press, New York (1972).
26. M.S. Blanter, I.S. Golovin, H. Neuhäuser, and R.-R. Sinning, *Internal Friction in Metallic Materials*: *A Handbook*, *Springer Series in Materials Science*, Springer (2007).
27. Z. Trojanová, V. Šíma, P. Lukáč, K. Halmešová, J. Džugan, and P. Minárik, *Crystals* **8**, 278 (2018).
28. A.V. Granato and K. Lücke, *J. Appl. Phys.* **27**, 789 (1956).
29. A.V. Granato and K. Lücke, *J. Appl. Phys.* **27**, 586 (1956).
30. A.V. Granato and K. Lücke, *J. Appl. Phys.* **52**, 7136 (1981).
31. F. Marchesoni and D. Segoloni, *Acta Physica Polonica B* **24**, 865 (1993).
32. Y. Cui, Y. Li, S. Sun, H. Bian, H. Huang, Z. Wang, Y. Koizumi, and A. Chiba, *Scripta Mater.* **101**, 8 (2015).
33. M.-H. Tsai, M.-H. Tsai, M.-S. Chen, L.-H. Lin, M.-H. Lin, C.-Z. Wu, K.-L. Ou, and C.-H. Yu, *J. Alloys Compd.* **509**, 813 (2011).
34. H. Watanabe, Y. Sasakura, N. Ikeo, and T. Mukai, *J. Alloys Compd*. **626**, 60 (2015).
35. D. Hou, T. Liu, L. Luo, L. Lu, H. Chen, and D. Shi, *Mater. Characterization* **124**, 122 (2017).
36. P. Klimanek and A. Pötzsch, *Mater. Sci. Eng. A* **324**, 145 (2002).
37. H.T. Huang, A. Godfrey, J.P. Zheng, and W. Liu, *Mater. Sci. Eng. A* **640**, 330 (2015).
38. P. Yang, Y. Yu, L. Chen, and W. Mao, *Scripta Mater.* **50**, 1163 (2014).
39. G.D. Fan, M.Y. Zheng, X.S. Hu, C. Xu, K. Wu, and I.S. Golovin, *J. Alloys Comp.* **549**, 38 (2013).
40. G.D. Fan, M.Y. Zheng, X.S. Hu, C. Xu, K. Wu, and I.S. Golovin, *Mater. Sci. Eng. A* **588**, 566 (2012).
41. Z. Trojanová, P. Lukáč, H. Ferkel, and W. Riehemann, *Mater. Sci. Eng. A* **370**, 154 (2004).

Амплітудно-залежне внутрішнє тертя в листах сплаву AZ31, підданих накопичувальному з'єднанню вальцюванням

Z. Trojanová, Z. Drozd, P. Lukáč, P. Minárik, J. Džugan, K. Halmešová

Дрібнозернисті листи магнієвих сплавів AZ31 були піддані накопичувальному з'єднанню вальцюванням (ARB). Після застосування ARB мікроструктура зразків ставала більш фрагментованою, і в листах спостерігалась яскраво виражена текстура. Амплітудно-залежне внутрішнє тертя (АЗВТ) вимірювали при кімнатній температурі. Зміни мікроструктури, такі як збільшення щільності дислокацій, зменшення розміру зерна, поява двійників та текстури, приводили до змін АЗВТ. Спостерігалась суттєва анізотропія вивчених властивостей. Експериментальні результати обговорюються на базі відомих фізичних механізмів, що відповідають за внутрішнє тертя.

Ключові слова: сплави магнію, накопичувальне з'єднання вальцюванням, внутрішнє тертя, дислокації, двійникування, текстура.

Амплитудно-зависимое внутреннее трение в листах сплава AZ31, подверженных накопительному соединению прокаткой

Z. Trojanová, Z. Drozd, P. Lukáč, P. Minárik, J. Džugan, K. Halmešová

Мелкозернистые листы магниевых сплавов AZ31 были подвергнуты накопительному соединению прокаткой (ARB). После применения ARB микроструктура образцов становилась более фрагментированной, и в листах наблюдалась ярко выраженная текстура. Амплитудно-зависимое внутреннее трение (АЗВТ) измеряли при комнатной температуре. Изменения микроструктуры, такие как увеличение плотности дислокаций, уменьшение размера зерна, появление двойников и текстуры, приводили к изменениям АЗВТ. Наблюдалась существенная анизотропия изученных свойств. Экспериментальные результаты обсуждаются на основе известных физических механизмов, отвечающих за внутреннее трение.

Ключевые слова: сплавы магния, накопительное соединение прокаткой, внутреннее трение, дислокации, двойникование, текстура.